Postprocessing of correlation for orientation estimation

Laurence G. Hassebrook, MEMBER SPIE
Michael E. Lhamon, MEMBER SPIE
Mao Wang
Jyoti P. Chatterjee
University of Kentucky
Department of Electrical Engineering
453 AH
Lexington, Kentucky 40506-0046
E-mail: lgh@engr.uky.edu

Abstract. We present a high-SNR approach to estimating the orientation of distorted target objects, where the distortion is out-of-plane rotation. The presence and position of the targets are detected with a bank of distortion-invariant correlation filters. The filter set we use, known as hybrid composite filters, yields complex responses at the target locations. The peak magnitude responses indicate target locations. The correlation phase angles, at the target locations, are linearly combined into complex signatures unique to a particular orientation. A maximum-likelihood M-ary classification algorithm is used to determine the most likely orientation from a finite number of orientations. In practice, we do not use all the hybrid filters and the ones we do use are optimally selected and combined for detection and discrimination. Given the target location, additional filtering can be accomplished with an inner-product operation rather than correlation. A second set of filters, optimized for angle estimation, are applied as inner products at the target locations to construct the orientation signatures. A rigorous mathematical treatment of the optimum signature detection architecture is presented and numerical simulations demonstrate the capabilities of this approach. [S0091-3286(97)00110-4]

Subject terms: correlation pattern recognition; distortion-invariant; correlation; filter banks; parameter estimation.

Paper CPR-01 received Feb. 11, 1997; revised manuscript received May 17, 1997; accepted for publication May 23, 1997. This paper is a revision of a paper presented at the SPIE conference on Optical Pattern Recognition VI, April 1995, Orlando, Florida. The paper presented there appears (unrefereed) in SPIE Proceedings Vol. 2490.

1 Introduction

We present a method of estimating the distortion parameter of an arbitrary input target from the complex correlation responses of a filter bank. The distortion parameter variation is represented by training set images, which in this case are distorted by out-of-plane rotation. It is assumed that the target class images reside in the same scene as the nontarget, or clutter, class images. We are not interested in the clutter class images so it is necessary to detect and locate the target class images while simultaneously discriminating clutter class objects. This detection and discrimination is performed in the presence of additive white Gaussian noise (AWGN), which is assumed to be sensor noise. Once the target is detected and located we element-wise multiply and integrate [i.e., the correlation is evaluated at one point by a vector inner-product (IP) result] a series of complex filter templates registered to the detected target image. For each filter IP, we have a single complex value, and these values are grouped in a vector representing a signature of the input image. The signature vector is then matched with possible response signature vectors and the IP match with the largest real component value indicates which distortion parameter, in this case a rotation angle, is most likely.

We limit our attention to distortion parameter estimation using model-based optical correlation filter designs.[1] Both parameter estimation and distortion-invariant object detection literature include hundreds of sources. Algorithms combined to form both object detection and orientation are less common and can be grouped into one of two categories, feature-based and correlation-based algorithms. The feature-based techniques reduce the problem dimensionality by operating on specific features. Examples of this include the determination and use of image boundaries[2–4] or special transformations.[5] Feature-based approaches can reduce the numerical burden of detection and estimation but usually require sophisticated algorithms, which are best implemented on general purpose computers. Correlation-based algorithms represent a simple approach[6] to detection and orientation estimation. However, correlation requires many low-level operations, which are best implemented on special purpose digital and optical processors. We limit out attention to distortion parameter estimation using model-based correlation filter designs.[1] We also limit our estimation to a finite number of rotations as represented by a training set. One of the most basic correlation approaches[6] to detection and parameter estimation is to correlate the input image with all the training images (in the form of matched filters). The problem with the matched filter approach is that it requires all training images to be correlated. By using complex distortion-invariant filters, the number of correlations is successively increased only until a desired performance measure is achieved rather than requiring all filters to be used.

 0091-3286/97/$10.00

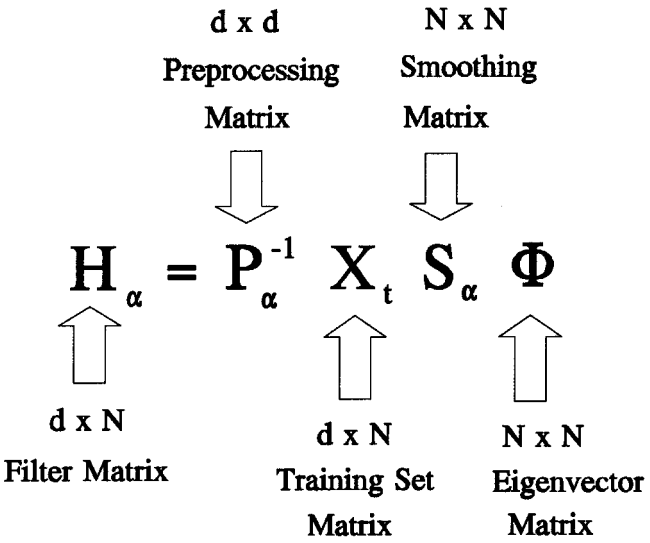

Fig. 1 HC filter design equation.

There are many distortion-invariant correlation filter designs[1] available for detection and location of input targets. We use hybrid composite (HC) filters[7] because these filters are representative of various other filter design types such as synthetic discriminant function[8] (SDF), minimum average correlation energy[9] (MACE), and linear phase Coefficient composite[10] (LPCC).

We give background on HC filters in Sec. 2. The parameter estimation theory is presented in Sec. 3. Optimal IP filter selection criteria are presented in Sec. 4. Results are given in Sec. 5 and conclusions are given in Sec. 6.

2 HC Filter Background

We detect, discriminate, and estimate rotation angle with a distortion-invariant correlation filter family known as HC filters.[7] In general, any method of detecting and discriminating the target will function, but to successively estimate the rotation angle we need an algorithm that uses the presence of the target to extract rotation information irrespective of rotation. We chose HC filter designs for this problem because their peak magnitude responses are distortion invariant, while the associated phase responses are sensitive to in-plane and/or out-of-plane rotation. Furthermore, since HC filters are a unification of classical SDF, MACE, and LPCC filter designs, our analysis is valid for these filter types as well. Figure 1 shows a diagram of the HC filter family matrix structure. The filter matrix contains, as its columns, N filter images, in lexicographic vector form. Each filter image contains d pixels. The HC matrix structure is centered around the target training set matrix, which has as its columns the training images in lexicographic form.

Preceding the training set matrix is the preprocessing matrix. The function of the preprocessing matrix is to modify the 2-D spectrum of the training set and thereby modify the intensity ''shape'' of the correlation plane and simultaneously modify the output noise response. For example, classical SDF filter design has a preprocessing matrix equivalent to an identity matrix, while MACE filter design has a preprocessing matrix that is approximately the training set spectrum. The SDF preprocessing matrix has no effect on the output correlation plane, while the MACE preprocessing matrix acts to prewhiten the input images, thereby making the output correlation shape be a sharp spike with suppressed sidelobes. The trade-off for the MACE preprocessing is high-frequency noise sensitivity. The HC filter preprocessing matrix allows for a transitional variation between the classical SDF and the MACE filter preprocessing matrix.

Immediately following the training set matrix, in Fig. 1, is the smoothing matrix. The function of this matrix is to linearly weight the training set as to achieve a specific response at the origin of the correlation plane given a specific input training image. Typically the more constrained the origin output response is, the less generalizable the filter is to images not in the training set. On the other hand, not enough constraint allows the output response to vary below the sidelobe response, thereby loosing both detection and discrimination ability. For example, the smoothing matrix acts to constrain the output origin responses to constant values for MACE and SDF designs. The result is loss in generalization and discrimination in both designs. On the other hand, the smoothing matrix is an identity matrix for LPCC filter design and imposes no constraint on the origin response. The result is improved, and more robust, detection, discrimination, and generalization performance for specific types of distortion, such as in-plane rotation. This improved performance, however, degrades gradually as the distortion becomes more generalized as in the case of out-of-plane rotation. By constraining the output responses using a smoothing matrix in transition between no constraints, as in LPCC filter design, and SDF/MACE filter constraints, the detection, discrimination, and generalization performance improves for all three filter types.

The last matrix in Fig. 1 is the eigenvector matrix. Its function is to expand what would be a single distortion-invariant filter into a family of filters. A family of filters allows the filter designer to isolate filtering properties, such as SNR and discrimination ability, better than if a single filter is used. This result becomes more pronounced when a filter bank of the most desired filters are used. Typically, filter banks have the advantage of attaining asymptotically improved results over an individual filter as the number of filters in the bank are increased. For example, with LPCC and HC filters, it was found that 3 filters significantly out performed a single filter. However, 10 filters did not significantly improve performance over 3 filters. Ideally, the last matrix is the eigenvector matrix of the training set correlation matrix where the magnitude values of the eigenvector matrix elements are constrained to unity. In HC filter design, this matrix is the discrete Fourier transform (DFT) or Fourier matrix where the elements are complex exponentials, linear in phase with respect to their element row/column index. Advantages of complex response values[11,12] as well as filter banks have been noted.[10,13–16]

The origin response to HC filters is complex, tends to have constant magnitude, and tends to be linear in phase with respect to the training image and filter order. If the constraints are made rigid, as in SDF or MACE filter designs, or if the training set has ideal cyclic properties, as in LPCC filter design, then the k'th order filter response at the origin to the n'th training image is

$$\lambda_{tt,k} \exp(-j2\pi kn/N) = \mathbf{x}_{t,n}^T \mathbf{h}_k^* . \quad (1)$$

The filter matrix structure, shown in Fig. 1, has a significance that goes beyond HC filter design. The HC matrix structure originated as a general matrix structure for SDF, minimum variance SDF (MVSDF) (Ref. 17), MACE, lock and tumbler[15] (LAT), LPCC, and linear phase response[10] (LPR) filter designs.[18] This structure is also valid for optimum trade-off,[19] GMACE (Ref. 20), minimum noise and correlation energy[21] (MINMACE), fractional power SDF (Ref. 22), and many other SDF filter designs. The individual matrix values vary among these filter designs, but the significance of the structure shown in Fig. 1 is that the function of the individual matrices are isolated. This functional isolation gives insight into the effects of the individual matrices on the filter performance, thereby enabling the filter designer to customize these effects to a specific application.

3 Parameter Estimation Theory and Architecture

We use correlation filters to detect and discriminate the target location from clutter images. Given the target location we implement IP filters to determine a response signature unique to a particular rotation. The IP filters are identical in design to HC correlation filters, but since the target location is known, a numerically efficient IP is performed either optically or electronically. An M-ary signature detector is used to determine the most likely rotation parameter. We develop the signature detector design for both additive colored Gaussian noise as well as for nonorthogonal IP filters. The general solution is simplified by assuming orthogonal filters and AWGN.

The input model is an additive Gaussian noise model such that for the n'th $d\times 1$ target training vector $\mathbf{x}_{t,n}$ we have

$$\mathbf{s}_n = \mathbf{x}_{t,n} + \mathbf{w}, \quad (2)$$

where $\mathbf{w}$ is assumed to be a spatially stationary zero-mean Gaussian noise vector. In general, the noise vector may be colored Gaussian noise.

The output response of the k'th order IP filter to an input $\mathbf{s}_n$ is

$$y(k) = \mathbf{s}_n^T \mathbf{h}_k^* = \lambda_{tt,k} \exp(-j2\pi kn/N) + \mathbf{w}^T \mathbf{h}_k^* , \quad (3)$$

where $y(k)$ is a complex random variable. By augmenting all the IP filter orders into a $d\times N$ matrix we obtain an $N\times 1$ signature vector $\mathbf{y}$ such that

$$\mathbf{y}_n^T = \mathbf{s}_n^T \mathbf{H}^* = \mathbf{x}_{t,n}^T \mathbf{H}^* + \mathbf{w}^T \mathbf{H}^* . \quad (4)$$

We design an M-ary maximum-likelihood (ML) detector that can determine which target response $\mathbf{y}_n$, out of the N possible responses, is present thereby determining the most likely rotation angle. The ML detector architecture is determined from the probability density functions associated with all possible response vectors. Since we assume a Gaussian process, we need only determine the mean vectors and covariance matrices for the N possible rotations. The mean vectors are given by

$$\boldsymbol{\mu}_n^T = E\{\mathbf{s}_n^T \mathbf{H}^*\} = \{\lambda_{tt,0}, \lambda_{tt,1} \exp(-j2\pi n/N), \ldots, \lambda_{tt,N-1} \times \exp[-j2\pi n(N-1)/N]\}. \quad (5)$$

The mean vector is used to determine the $N\times N$ covariance matrix as

$$\mathbf{C}_{yy} = E[(\mathbf{y}_n - \boldsymbol{\mu}_n)^*(\mathbf{y}_n - \boldsymbol{\mu}_n)^T] = E[(\mathbf{H}^T\mathbf{w})(\mathbf{w}^T\mathbf{H}^*)] = \mathbf{H}^T \mathbf{C}_{ww} \mathbf{H}^*, \quad (6)$$

where

$$\mathbf{C}_{ww} = E(\mathbf{w}\mathbf{w}^T). \quad (7)$$

The covariance matrix $\mathbf{C}_{yy}$ is independent of the distortion parameter. Given that A_t is the condition that a target is present and n indicates that the n'th target is present, the multivariate conditional probability density function (pdf) is

$$P_{y|n,A_t}(\mathbf{y}|n,A_t) = \frac{1}{(2\pi)^{N/2}|\mathbf{C}_{yy}|^{1/2}} \times \exp[-\tfrac{1}{2}(\mathbf{y}-\boldsymbol{\mu}_n)^T \mathbf{C}_{yy}^{-1}(\mathbf{y}-\boldsymbol{\mu}_n)^*]. \quad (8)$$

Thus if we can detect which target is present, then we also know the rotation parameter. The maximum pdf value for a given input determines which target is actually present. This decision process does not change if we take the log of the pdf's since the log is a monotonic function. Since the covariance matrix is common to all rotations we can ignore the coefficient in Eq. (8) and concentrate on the exponent, which is the result of the log operation. By removing constant terms, which are independent of rotation, the decision function for the n'th rotation is

$$G_{A,n} = \mathscr{R}\{\mathbf{y}^T \mathbf{C}_{yy}^{-1} \boldsymbol{\mu}_n^*\} - \tfrac{1}{2}\boldsymbol{\mu}_n^T \mathbf{C}_{yy}^{-1} \boldsymbol{\mu}_n^* , \quad (9)$$

where $\Re\{\}$ indicates the real component.

The linear architecture, shown in Eq. (9), is optimum in minimum probability of error (MPE) for both colored Gaussian noise and nonorthogonal filters. The angle selection is based on the maximum G_n for $n=0,1,\ldots,(N-1)$. The architecture in Eq. (9) is simplified even further by assuming orthogonal filters and white Gaussian noise. If the filters are orthogonal, the covariance matrix is diagonal and if the noise is white Gaussian then the input noise covariance matrix is proportional to an identity matrix. Making the assumption of orthogonal filters, but allowing for colored noise, we obtain

$$G_{B,n} = \Re\left\{\sum_{k=0}^{N-1} \frac{1}{c_k} y(k) \boldsymbol{\mu}_n^*(k)\right\} - \frac{1}{2}\sum_{k=0}^{N-1} \frac{\lambda_{tt,k}^2}{c_k}, \quad (10)$$

where the signature covariance matrix is $\mathbf{C}_{yy} = \mathrm{diag}\{c_0, c_1, \ldots, c_{N-1}\}$.

On the other hand, if we assume nonorthogonal filters and AWGN, the signature measure is

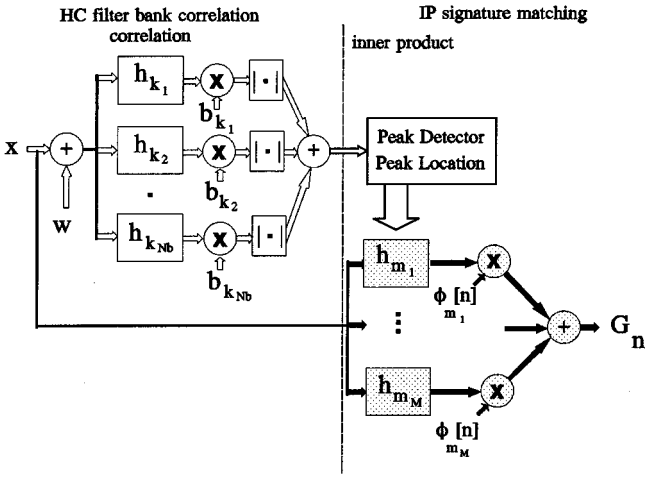

Fig. 2 Target detection, discrimination, and angle estimation architecture. The HC architecture is used to locate the target using correlation. The signature matching is accomplished using IP operations.

$$G_{C,n}=\Re\{\mathbf{y}^T(\mathbf{H}^T\mathbf{H}^*)^{-1}\boldsymbol{\mu}_n^*\}-\tfrac{1}{2}\boldsymbol{\mu}_n^T(\mathbf{H}^T\mathbf{H}^*)^{-1}\boldsymbol{\mu}_n^*, \tag{11}$$

where the constant coefficient from the noise covariance will not affect the detection so it is discarded.

If both the filters are orthogonal and the noise is AWGN the signature covariance matrix becomes

$$\mathbf{C}_{yy}=\frac{\sigma^2}{d}\,\mathbf{H}^T\mathbf{H}^*=\frac{N\sigma^2}{d}\,\boldsymbol{\Lambda}_{tt}, \tag{12}$$

where $\Lambda_{tt}=\mathrm{diag}\{\lambda_{tt,0},\lambda_{tt,1},\ldots,\lambda_{tt,N-1}\}$. Ignoring the constant coefficient of the signature covariance matrix and the sum of all eigenvalues, which are the same for all signatures, we have the ML signature measure defined as

$$G_n=\Re\left\{\sum_{k=0}^{N-1} y(k)\,\exp\,(j2\pi kn/N)\right\}$$
$$=\Re\left\{\sum_{k=0}^{N-1} y(k)\,\boldsymbol{\phi}_n^*(k)\right\}=\Re\{\mathbf{y}^T\boldsymbol{\phi}_n^*\}, \tag{13}$$

where $\boldsymbol{\phi}_k$ is an $N\times 1$ Fourier vector. The entire HC filter bank and IP architecture, given in Eq. (13), is shown in Fig. 2.

4 Optimum IP Filter Selection

In practice, not all the IP filters would be selected. Which IP filters to be used in the angle estimation is determined by their associated SNR as well as their ambiguity. Since the target is already located, clutter discrimination is not a criterion for the IP filter selection. However, SNR is an important selection criterion. We develop a signature detection criterion for optimum SNR as a function of IP filter orders. The IP filters with the largest magnitude response yield the largest SNR and are selected first for maximum signature detection SNR. To simplify the derivation, we assume that the distortion is ideally cyclic, resulting in orthogonal IP filters, and the noise is AWGN. In Sec. 4.1, we derive the signal energy. In Sec. 4.2 we derive the noise energy and combine it with the signal energy for a SNR measure. The IP filters with the highest individual SNR are selected first and yield the highest signature detection SNR. However, SNR cannot be the only criterion for filter selection because certain IP filter orders would yield ambiguous results. In Sec. 4.3, IP filter ambiguity is considered as well as SNR to obtain an optimized filter selection criterion.

4.1 *Signature Signal Energy*

The target image input is assumed to be deterministic so that the maximum signature energy is defined as the square of Eq. (13) such that

$$G_n^2=\Re\{\mathbf{y}_n^T\boldsymbol{\phi}_n^*\}^2=\Re\{\mathbf{x}_{t,n}^T\mathbf{H}^*\boldsymbol{\phi}_n^*\}^2, \tag{14}$$

where we assume cyclic distortion so the IP filter matrix is equivalent to the LPCC filter matrix such that

$$\mathbf{H}^*=\mathbf{X}_t\boldsymbol{\Phi}, \tag{15}$$

and the response to a single input is

$$\mathbf{y}_n^T=\boldsymbol{\mu}_n^T=\boldsymbol{\phi}_n^T\boldsymbol{\Lambda}_{tt}. \tag{16}$$

Thus, the signature energy is

$$G_n^2=\Re\{\boldsymbol{\phi}_n^T\boldsymbol{\Lambda}_{tt}\boldsymbol{\phi}_n^*\}^2=\left(\sum_{k=0}^{N-1}\lambda_{tt,k}\right)^2=N^2. \tag{17}$$

For cyclic distortion and N odd we know $\lambda_{tt,n}=\lambda_{tt,N-n}$. If we select a subset of all possible IP filters, the signature energy is

$$G_n^2=\left(\lambda_{tt,0}+2\sum_{k=1}^{N_b-1}\lambda_{tt,k}\right)^2\leqslant N^2, \tag{18}$$

where $N_b\leqslant(N+1)/2$.

4.2 *Signature Noise Energy and SNR*

The signature noise ''energy'' is defined as the signature variance when the IP filter bank has AWGN as its input. The noise is assumed to be zero mean AWGN in a vector form. The noise energy, that is the variance, of the signature detector is given by

$$E(G_n^2)=E(\Re\{\mathbf{y}^T\boldsymbol{\phi}_n^*\}^2)=E\left[\Re\left\{\sum_{k=0}^{N-1}\mathbf{y}(k)\,\boldsymbol{\phi}_n^*(k)\right\}^2\right], \tag{19}$$

where $\mathbf{y}^T=\mathbf{w}^T\mathbf{H}^*$.

The same assumptions are made of cyclic distortion with the IP filter subset, as for the signal energy. The noise variance in each signature measure is given by

$$E\{G_{n,N_b}^2\}=E\left\{\left[\mathbf{y}(0)+2\sum_{k=1}^{N_b-1}\Re\{\mathbf{y}(k)\,\boldsymbol{\phi}_n^*(k)\}\right]^2\right\}. \tag{20}$$

By substituting the identity

$$\Re\{A\}=\frac{A+A^*}{2}, \tag{21}$$

into Eq. (20), multiplying out the square, and bringing the expected value function around only the random variables yields

$$\begin{aligned}E(G_{n,N_b}^2)=&E[\mathbf{y}^2(0)]+2\sum_{k=1}^{N_b-1}\{E[\mathbf{y}(0)\mathbf{y}(k)]\boldsymbol{\phi}_n^*(k)\\&+E[\mathbf{y}(0)\mathbf{y}^*(k)]\boldsymbol{\phi}_n(k)\}\\&+\sum_{k=1}^{N_b-1}\sum_{u=1}^{N_b-1}\{E[\mathbf{y}(k)\mathbf{y}(u)]\boldsymbol{\phi}_n^*(k)\boldsymbol{\phi}_n^*(u)\\&+E[\mathbf{y}(k)\mathbf{y}^*(u)]\boldsymbol{\phi}_n^*(k)\boldsymbol{\phi}_n(u)\}\\&+\sum_{k=1}^{N_b-1}\sum_{u=1}^{N_b-1}\{E[\mathbf{y}^*(k)\mathbf{y}(u)]\boldsymbol{\phi}_n(k)\boldsymbol{\phi}_n^*(u)\\&+E[\mathbf{y}^*(k)\mathbf{y}^*(u)]\boldsymbol{\phi}_n(k)\boldsymbol{\phi}_n(u)\}.\end{aligned} \tag{22}$$

The expectation in the first term of Eq. (22) yields

$$\begin{aligned}E[\mathbf{y}^2(0)]&=E(\mathbf{w}^T\mathbf{h}_0^*\mathbf{w}^T\mathbf{h}_0^*)=\mathbf{h}_0^HE(\mathbf{w}\mathbf{w}^T)\mathbf{h}_0^*=\mathbf{h}_0^H\mathbf{C}_{ww}\mathbf{h}_0^*\\&=\frac{\sigma^2}{d}\,\mathbf{h}_0^H\mathbf{h}_0^*=\frac{\sigma^2}{d}\,\boldsymbol{\phi}_0^T\mathbf{X}_t^T\mathbf{X}_t\boldsymbol{\phi}_0=\frac{\sigma^2}{d}\,\boldsymbol{\phi}_0^T\mathbf{R}_{tt}\boldsymbol{\phi}_0\\&=\frac{\sigma^2\lambda_{tt,0}}{d}\,\boldsymbol{\phi}_0^T\boldsymbol{\phi}_0=\frac{\sigma^2N\lambda_{tt,0}}{d}.\end{aligned} \tag{23}$$

The expectations in the second and third terms of Eq. (22) yield

$$\begin{aligned}E[\mathbf{y}(0)\mathbf{y}(k)]&=E[\mathbf{y}(0)\mathbf{y}^*(k)]=\mathbf{h}_0^HE(\mathbf{w}\mathbf{w}^T)\mathbf{h}_k=\mathbf{h}_0^H\mathbf{C}_{ww}\mathbf{h}_k\\&=\frac{\sigma^2}{d}\,\mathbf{h}_0^H\mathbf{h}_k=\frac{\sigma^2}{d}\,\boldsymbol{\phi}_0^T\mathbf{R}_{tt}\boldsymbol{\phi}_k^*=\frac{\sigma^2\lambda_{tt,k}}{d}\,\boldsymbol{\phi}_0^T\boldsymbol{\phi}_k^*\\&=\frac{\sigma^2N\lambda_{tt,0}}{d}\,\delta(k).\end{aligned} \tag{24}$$

The expectations in the fourth and seventh terms of Eq. (22) yield

$$\begin{aligned}E[\mathbf{y}(k)\mathbf{y}(u)]&=E[\mathbf{y}^*(k)\mathbf{y}^*(u)]=\mathbf{h}_k^H\mathbf{C}_{ww}\mathbf{h}_u^*=\frac{\sigma^2}{d}\,\mathbf{h}_k^H\mathbf{h}_u^*\\&=\frac{\sigma^2}{d}\,\boldsymbol{\phi}_k^T\mathbf{R}_{tt}\boldsymbol{\phi}_u=\frac{\sigma^2\lambda_{tt,u}}{d}\,\boldsymbol{\phi}_k^T\boldsymbol{\phi}_u\\&=\frac{\sigma^2\lambda_{tt,u}}{d}\,\boldsymbol{\phi}_k^T\boldsymbol{\phi}_{N-u}^*\\&=\frac{\sigma^2N\lambda_{tt,u}}{d}\,\delta[k-(N-u)].\end{aligned} \tag{25}$$

The expectations in the fifth and sixth terms of Eq. (22) yield

$$\begin{aligned}E[\mathbf{y}(k)\mathbf{y}^*(u)]&=E[\mathbf{y}^*(k)\mathbf{y}(u)]=\mathbf{h}_k^T\mathbf{C}_{ww}\mathbf{h}_u^*=\frac{\sigma^2}{d}\,\mathbf{h}_k^T\mathbf{h}_u^*\\&=\frac{\sigma^2}{d}\,\boldsymbol{\phi}_k^H\mathbf{R}_{tt}\boldsymbol{\phi}_u=\frac{\sigma^2\lambda_{tt,u}}{d}\,\boldsymbol{\phi}_k^H\boldsymbol{\phi}_u\\&=\frac{\sigma^2N\lambda_{tt,u}}{d}\,\delta(k-u).\end{aligned} \tag{26}$$

By incorporating the resulting identities from Eqs. (23) through (26) into Eq. (22) we obtain the noise variance as

$$\begin{aligned}E(G_{n,N_b}^2)=\frac{\sigma^2N}{d}\Bigg\{&\lambda_{tt,0}+2\sum_{k=1}^{N_b-1}\lambda_{tt,0}\delta[k]\boldsymbol{\phi}_n^*(k)\\&+2\sum_{k=1}^{N_b-1}\lambda_{tt,0}\delta[k]\boldsymbol{\phi}_n(k)+\sum_{k=1}^{N_b-1}\sum_{u=1}^{N_b-1}\lambda_{tt,k}\\&\times\delta[k-(N-u)]\boldsymbol{\phi}_n^*(k)\boldsymbol{\phi}_n^*(u)\\&+\sum_{k=1}^{N_b-1}\sum_{u=1}^{N_b-1}\lambda_{tt,k}\delta[k-u]\boldsymbol{\phi}_n^*(k)\boldsymbol{\phi}_n(u)\\&+\sum_{k=1}^{N_b-1}\sum_{u=1}^{N_b-1}\lambda_{tt,k}\delta[k-u]\boldsymbol{\phi}_n(k)\boldsymbol{\phi}_n^*(u)\\&+\sum_{k=1}^{N_{b-1}}\sum_{u=1}^{N_b-1}\lambda_{tt,k}\delta[k-(N-u)]\boldsymbol{\phi}_n(k)\boldsymbol{\phi}_n(u)\Bigg\}.\end{aligned} \tag{27}$$

In Eq. (27) the second and third terms go to zero because the range of k in the summation never has value of zero, thus the $\delta[\ ]$ function is always zero. Similarly in the fourth and last term k is never equal to $N-u$, thus the $\delta[\ ]$ function is always zero. The only remaining terms are therefore the first, fifth, and sixth. The fifth and sixth terms are identical so they can be added together and reduced to a single summation due to the $\delta[\ ]$ function. The noise energy in each signature measure is identical and can be written as a function of the number of IP filters included in the IP filter bank as

$$E(G_{n,N_b}^2)=\frac{\sigma^2N}{d}\left(\lambda_{tt,0}+2\sum_{k=1}^{N_b-1}\lambda_{tt,k}\right)\leqslant\frac{\sigma^2N^2}{d}, \tag{28}$$

where the equality holds for $N_b=(N+1)/2$ and N is odd.

The SNR ratio, which is Eq. (18) divided by Eq. (28), is maximized by including the IP filters with the largest eigenvalues. The bounded signature measure SNR is given by

$$\begin{aligned}\mathrm{SNR}_G(N_b)&=\frac{d}{\sigma^2N}\left(\lambda_{tt,0}+2\sum_{k=1}^{N_b-1}\lambda_{tt,k}\right)\\&\leqslant\frac{d}{\sigma^2N}\sum_{k=0}^{N_b-1}g_k\lambda'_{tt,k}\leqslant\frac{d}{\sigma^2},\end{aligned} \tag{29}$$

where

$$g_k=\begin{cases}1 & \text{for } \lambda'_{tt,k}=\lambda_{tt,0}\\ 2 & \text{else}\end{cases}, \tag{30}$$

and the primed eigenvalues represent the sorted eigenvalues such that

$$\lambda'_{tt,0}\geqslant\lambda'_{tt,1}\geqslant\cdots\geqslant\lambda'_{tt,N_b-1}. \tag{31}$$

Equality is achieved, in Eq. (29) when $N_b=(N+1)/2$.

4.3 *IP Filter Ambiguity*

If SNR is the only criterion used to select IP filters, the resulting signature matching may be ambiguous. This ambiguity is due to the elements of the signature being complex phasor terms. That is, a single set of phase angles may be associated with several possible rotations. For example, the zero-order IP filter $\mathbf{h}_0$ has the same response magnitude and phase for all input rotations yet typically has the highest SNR. Thus the zero-order IP filter yields completely ambiguous results. On the other hand, the first-order IP filter $\mathbf{h}_1$ has a unique phase associated with all rotation angles. The first-order filter has no ambiguity but does not typically have the highest SNR. Higher order filters have increasing ambiguity and their interaction as a signature can become complicated. For these reasons, we have chosen a practical compromise to the filter selection. We treat the zero-order filter as the least desirable filter and the first-order IP filter as the most desirable filter to be selected. All other filters are selected by the SNR value. Our results support this selection criterion as requiring less filters than using the either SNR or ordering criterions alone.

5 Numerical Results

We test the combined as well as the individual component performance of the HC/IP-filter-based detection, discrimination, and angle estimation system. Two signature detectors are used, one given in Eq. (11) is optimized for orthogonal filters and the other, given in Eq. (13), is optimum for orthogonal filters. Both signature detectors are optimized for AWGN. The input data consists of 36 binary images of numerically simulated aircraft silhouettes. There are four different aircraft types, one aircraft type is the target class and the other three types are the clutter class. Both target and clutter aircraft are uniformly rotated from 0 to 360 deg and viewed 45 deg from the perpendicular. Technically, we refer to this problem as a single parameter, 45-deg out-of-plane rotation distortion. Only the target training set is used in the filter design, no clutter information is used. The HC correlation filter bank consists of filters whose weighting and design are based on to previous work.[7] The IP filters were created and selected as described in this research. There are four experiments.

The first experiment demonstrates the detection, discrimination, and estimation capability without noise. In Fig. 3 we show a sample 128-$\times$128-pixel test image. The aircraft in the lower left is the target SMPR. The clutter class includes the Phantom (lower right), B-747 (upper right) and the F-104 (upper left). We found the target and clutter peak intensities for the 36 test inputs and formed a histogram of the response distribution. In Fig. 4 we show a peak response distribution of a three-filter HC filter bank. The graph shows the distribution for 36 clutter and 34 target responses. Two of the target responses are not shown because they are outside the upper range of the histogram. Note the large thresholding window between intensities 0.4 and 0.8. Thus, even though the target intensity has a large spread, there is clearly enough window region to achieve 0 MPE. All targets were exactly located and only two IP filters were required to exactly estimate the rotation angle index.

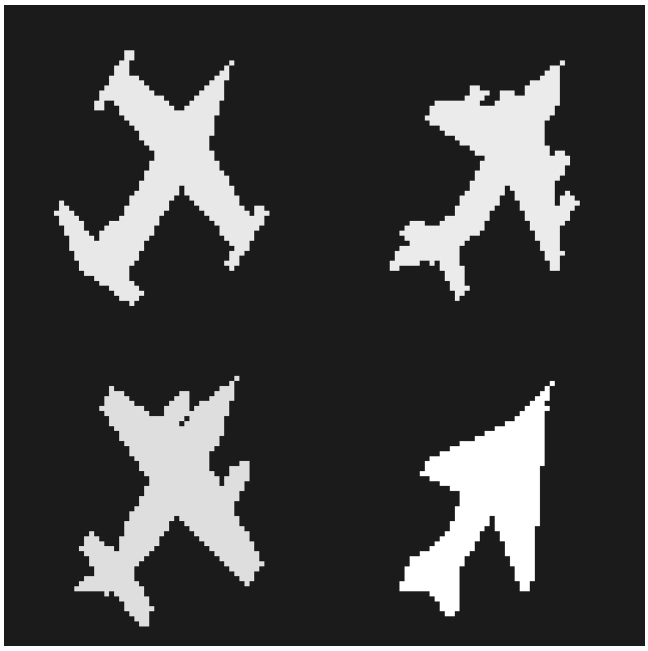

Fig. 3 Sample 128$\times$128 input test image. Target aircraft SMPR (lower left). Clutter images are Phantom (lower right), B-747 (upper right), and F-104 (upper left).

The second experiment is the same as the first experiment except that the input test images are corrupted by AWGN as shown in Fig. 5. The noise energy is equal to the signal energy for an input SNR$=1=10\log(1)=0$ dB. The system functions with 0% probability of error in classifica-

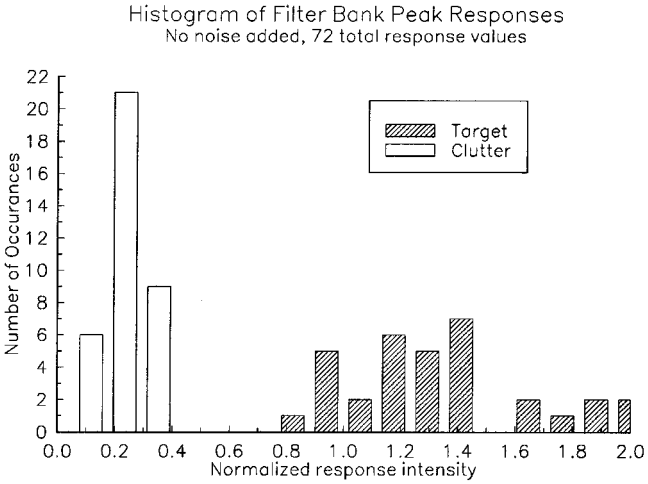

Fig. 4 Histogram of peak intensity responses for 36 test images with no noise.

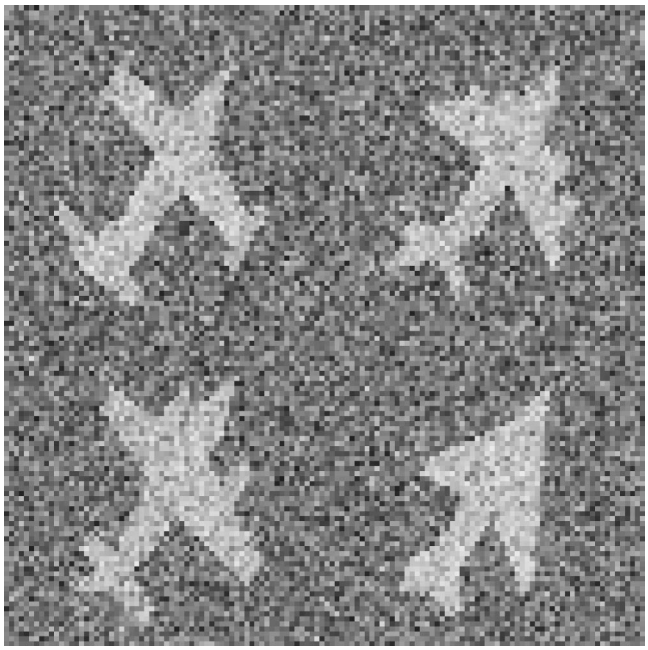

Fig. 5 Sample 128×128 input test image with 0-dB SNR. Noise is AWGN and the aircraft types are the same as described in Fig. 3.

tion, 0% error in location of the target, and requires only two IP filters to achieve 0% error in angle estimation. The target and clutter distribution for a three-filter HC filter bank is shown in Fig. 6. The threshold window decreases to between 0.6 and 0.9, which is still adequate for 0-MPE discrimination. Detection and location of the target are exact and the Gaussian shape, due to noise, is apparent in Fig. 6. The mean squared error (MSE) in the estimated angle index (0 to 35 representing 0 to 350 deg) is in included in Fig. 7. The estimate was performed twice, once by assuming the filters are orthogonal and once using their actual nonorthogonal relationship. A comparison of these two detectors is shown in Fig. 7. For this experiment, the number of filters needed for 0% error were two IP filters.

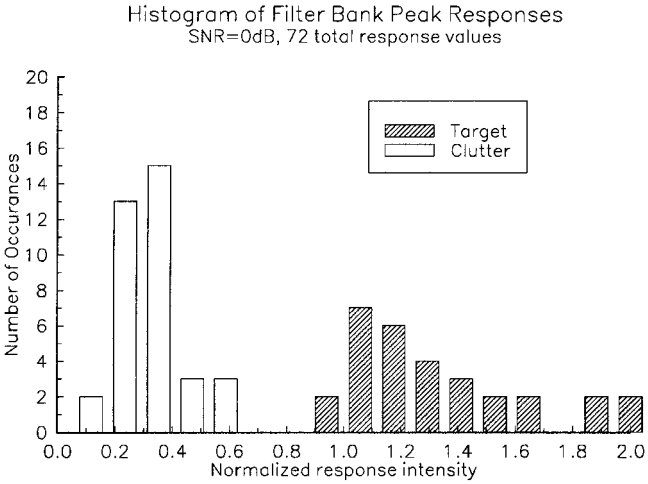

Fig. 6 Histogram of peak intensity responses for 36 test images with 0-dB SNR.

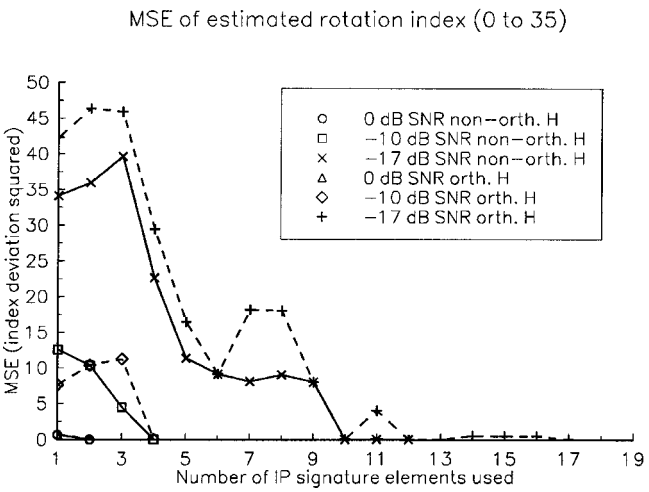

Fig. 7 MSE of index estimation for the IP signature detector. The horizontal axis indicates how many IP filters are used for detection. There are 36 signatures used. Curves are for 0-dB SNR, −10-dB SNR, and −17-dB SNR. For the −17-dB SNR case, the correct target locations are known.

The third experiment is the same as the second experiment except that the noise energy is 10 times more than the signal energy such that $\mathrm{SNR} = 0.1 = 10 \log(0.1) = -10$ dB. An example test image is shown in Fig. 8. The target is still located with 0% error but 15 HC filters are required and the discrimination ability of the HC filter bank between target and clutter begins to degrade, as shown in Fig. 9 Both IP signature detectors still perform well, as shown by the curves in Fig. 7, but both require four IP filters.

The fourth experiment is the same as the third experiment except that we test only the estimation component of

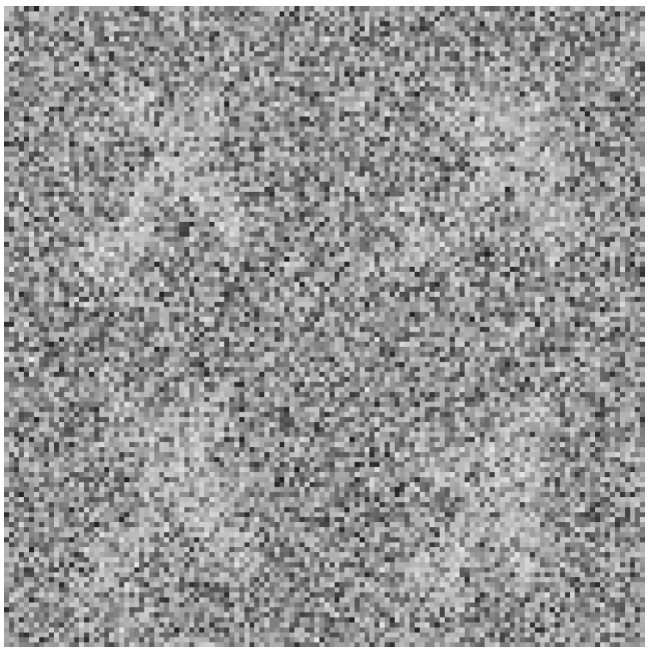

Fig. 8 Sample 128×128 input test image with −10-dB SNR. Noise is AWGN and the aircraft types are the same as described in Fig. 3.

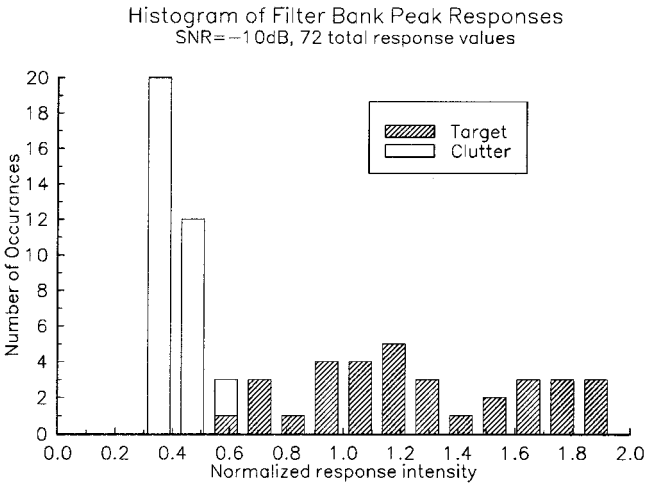

Fig. 9 Histogram of peak intensity responses for 36 test images with −10-dB SNR.

the system. The SNR is $1/50 = 10 \log (1/50) = -17$ dB. In this case, the detection and discrimination ability of the correlation component have completely degraded to the point of unreliable target location, but the signature detection continues to function given correct target locations. The curves in Fig. 7 show that the MSE of the angle estimation goes almost to 0 with 12 IP filters, given correct target locations and the orthogonal signature detector. The MSE goes to 0 with 11 IP filters for the nonorthogonal detector and it is apparent from the curves that the nonorthogonal detector has consistently lower MSE than the orthogonal detector design.

6 Conclusions

We present a new technique for estimating the distortion parameter based on IP operations. We used rotation estimation as an example but because of the IP filter design, the technique can be extended to general distortion parameter estimation. The IP filter response signature matching is optimized for both nonorthogonal filters and colored noise. We developed IP filter selection criterion, optimal in SNR, given orthogonal IP filters, and an AWGN input model. The resulting system was robust for noisy images. At 0-dB input SNR we could detect, discriminate, and estimate the angle with 3 correlation filters and 2 IP filters. At −10-dB input SNR, we could detect, discriminate, and estimate the angle with 15 correlation filters, and 4 IP filters. At −17-dB input SNR, we lost our ability to detect and discriminate accurately, but if we could locate the input targets, then the IP filter estimation could estimate with 0% error with 12 IP filters. We eliminated ambiguity by simply forcing the first IP filter selected to be the one filter with no ambiguities and the last IP filter to be the one with maximum ambiguity. All filters in between were selected for maximum SNR. We believe that these results indicate a new and robust method for distortion parameter estimation.

Acknowledgments

This research was supported through the National Aeronautics and Space Administration Cooperative Agreement No. NCCW-60.

References

1. B. V. K. Vijaya Kumar, ''Tutorial survey of composite filter designs for optical correlators,'' *Appl. Opt.* **31**(23), 4773–4800 (1992).
2. D. Cyganski and R. F. Vaz, ''Linear signal decomposition approach to affine invariant contour identification,'' *Pattern Recog.* **28**(12), 1845–1853 (1995).
3. M. Wang, L. G. Hassebrook, J. Kirsch, J. Evans, and C. Knapp, ''Active image registration and recognition,'' *Proc. SPIE* **2488**(5), 385–395 (1995).
4. M. Wang, J. Evans, L. G. Hassebrook, and C. Knapp, ''A multi-stage, optimal active contour,'' *IEEE Trans. Image Process.* **5**(11), 1586–1591 (1996).
5. X. Lou, L. G. Hassebrook, M. Lhamon, and J. Li, ''Numerically efficient angle, width, offset and discontinuity estimation of lines using the discrete Fourier-bilinear transformation,'' *IEEE Trans. Image Process.* (October 1997).
6. H. L. Van Trees, *Detection, Estimation and Modulation Theory: Part I*, Wiley, New York (1968).
7. L. G. Hassebrook, M. Rahmati, and B. V. K. Vijaya Kumar, ''Hybrid composite filter banks for distortion-invariant optical pattern recognition,'' *Opt. Eng.* **31**, 923–933 (1992).
8. C. F. Hester and D. Casasent, ''Multivariant technique for multi-class pattern recognition,'' *Appl. Opt.* **19**, 1758–1761 (1980).
9. A. Mahalanobis, B. V. K. Vijaya Kumar, and D. Casasent, ''Minimum average correlation energy filters,'' *Appl. Opt.* **26**, 3633–3640 (1987).
10. L. G. Hassebrook, B. V. K. Vijaya Kumar, and L. Hostetler, ''Linear phase coefficient composite filters for distortion-invariant optical pattern recognition,'' *Opt. Eng.* **29**, 1033–1043 (1990).
11. B. V. K. Vijaya Kumar, Z. Bahri, and A. Mahalanobis, ''Constraint phase optimization in minimum variance synthetic discriminant functions,'' *Appl. Opt.* **27**, 409–413 (1988).
12. B. V. K. Vijaya Kumar, J. D. Brasher, C. F. Hester, G. Srinivasan, and S. Bollapragada, ''Synthetic discriminant functions for recognition of images on the boundary of the convex hull of the training set,'' *Pattern Recog.* **27**(4), 543–548 (1994).
13. Y. Hsu, H. H. Arsenault, ''Statistical performance of the circular harmonic filter for rotation-invariant pattern recognition,'' *Appl. Opt.* **22**(18), 2804–2809 (1983).
14. R. R. Kallman, ''The construction of low noise optical correlation filters,'' *Appl. Opt.* **25**, 1032–1033 (1986).
15. G. F. Schils and D. W. Sweeney, ''An optical processor for recognition of 3-D targets viewed from any direction,'' *J. Opt. Soc. Am. A* **5**, 1309–1321 (1988).
16. R. Wu and H. Stark, ''Three dimensional object recognition from multiple views,'' *J. Opt. Soc. Am. A* **3**, 1543–1557 (1986).
17. B. V. K. Vijaya Kumar, ''Minimum variance synthetic discriminant functions,'' *J. Opt. Soc. Am. A* **3**, 1579–1584 (1986).
18. L. G. Hassebrook, ''Design of distortion-invariant linear phase response correlation filters and filter banks,'' PhD Dissertation, Carnegie Mellon University (July 1990).
19. P. Refregier, ''Filter design for optical pattern recognition: multicriteria optimization approach,'' *Opt. Lett.* **15**(15), 854–856 (1990).
20. D. Casasent, G. Ravichandran, and S. Bollapraggada, ''Gaussian MACE correlation filters,'' *Appl. Opt.* **30**, 5176–5181 (1991).
21. G. Ravichandran and D. Casasent, ''Minimum noise and correlation energy (MINMACE) optical correlation filter,'' *Appl. Opt.* **31**, 1823–1833 (1992).
22. J. D. Brasher and J. M. Kinser, ''Fractional-power synthetic discriminant functions,'' *Pattern Recog.* **27**(4), 577–585 (1994).

Laurence G. Hassebrook received his BSEE degree from the University of Nebraska in Lincoln in 1979, his MSEE degree from Syracuse University in 1987, and his PhD in electrical and computer engineering from Carnegie Mellon University in 1990. He worked at Lincoln Electric System Corporation from 1980 to 1981 in development and automation of load analysis systems. From 1981 to 1984 and then during summer from 1985 through 1987, he worked in non-destructive testing and inspection at IBM Corporation in Endicott, New York. He is presently an associate

professor of electrical engineering at the University of Kentucky. His interests are in the area of 3-D data acquisition, pattern recognition, and opto-electronic signal processing.

Michael E. Lhamon received his BSEE degree from Ohio Northern University in 1990, his MSEE from Georgia Institute of Technology in 1991, and his PhD from the University of Kentucky in 1997. He worked for the National Radio Astronomy Observatory at the Very Large Array in Socorro, New Mexico, during 1989 and 1990 and Multi-Link Incorporated in 1992. His present interests include automatic object recognition and discrimination and real-time digital and optical signal processing. Additional interests include real-time distributed processing on parallel digital signal processors and field programmable gate arrays. He is a member of SPIE and IEEE.

Mao Wang received his BS degree and MS degree in electrical engineering from Nanjing Institute of Technology in 1984 and 1987, respectively. He received his MS degree in biomedical engineering in 1992 and his PhD degree in electrical engineering in 1995 from the University of Kentucky. He is currently a lead engineer at Motorola Cellular Infrastructure Group, Arlington Heights, Illinois. His research interests include digital signal and imaging processing and digital communications.

Jyoti P. Chatterjee received his BE in electronics engineering from Visvesvaraya Regional College of Engineering, India, in 1990. After completing his BE degree he worked with Godrej & Boyce Manufacturing Company, India, from 1990 through 1993 as a service executive. He received his MS in electrical engineering from the University of Kentucky in 1996. Since then he has been employed at Digital Technics Incorporated, Maryland, as a DSP software engineer.